


Rotation-driven transition into coexistent Josephson modes in an atomtronic dc superconducting quantum interference device

D. M. Jezek and H. M. Cataldo *IFIBA-CONICET and Departamento de Física, FCEN-UBA Pabellón 1, Ciudad Universitaria, 1428 Buenos Aires, Argentina* (Received 30 August 2021; revised 7 November 2021; accepted 8 November 2021; published 22 November 2021)

By means of a two-mode model, we show that transitions to different arrays of coexistent regimes in the phase space can be attained by rotating a double-well system, which consists of a toroidal condensate with two diametrically placed barriers. Such a configuration corresponds to the atomtronic counterpart of the well-known direct-current superconducting quantum interference device. Due to the phase gradient experimented by the on-site localized functions when the system is subject to rotation, a phase difference appears on each junction in order to satisfy the quantization of the velocity field around the torus. We demonstrate that such a phase can produce a significant change on the relative values of different types of hopping parameters. In particular, we show that within a determined rotation frequency interval a hopping parameter, usually disregarded in nonrotating systems, turns out to rule the dynamics. At the limits of such a frequency interval, bifurcations of the stationary points occur, which substantially change the phase-space portrait that describes the orbits of the macroscopic canonical conjugate variables. We analyze the emerging dynamics that combines the zero and π Josephson modes, and evaluate the small-oscillation time periods of such orbits at the frequency range where each mode survives. All the findings predicted by the model are confirmed by Gross-Pitaevskii simulations.

DOI: [10.1103/PhysRevA.104.053319](https://doi.org/10.1103/PhysRevA.104.053319)

I. INTRODUCTION

Much interest has been devoted in recent years to Bose-Einstein condensates confined by toroidal traps radially crossed by a number of rotating barriers, as such configurations present the clear potential of becoming central building blocks for future atomtronic devices [1]. In case of a single rotating barrier, which yields the cold atom analog of the celebrated rf superconducting quantum interference device (SQUID)—a superconducting ring interrupted by a Josephson junction [2]—well-defined phase slips between quantized persistent currents have been observed [3], along with a quantized hysteresis behavior [4]. The case of two diametrically disposed barriers corresponds to the cold atom version of the dc SQUID [2], perhaps the most sensitive detector for magnetic flux available today. We may denote such atomtronic counterparts of SQUIDs as atomtronic quantum interference devices (AQUIDs) [1]. In a SQUID, a current flow is established by changing the magnetic flux through the loop, whereas the same effect in an AQUID is obtained as a consequence of the barrier rotation, or, equivalently, by imparting a geometric phase directly to the atoms via suitably designed laser fields [5]. This makes rotation sensing possible, as already demonstrated for neutral atoms of superfluid helium [6] and very recently for ultracold atoms [7], where the quantum interference of currents in a dc AQUID was observed. Such efforts, along with other recent proposals to achieve rotation sensing by atomic persistent currents [8–10], may be considered as part of the rapidly growing branch of research known as “quantum sensing” [11].

Previously, Josephson effects [12] and resistive flows [13] had also been observed in dc AQUIDs. On the other hand, a

variant of rf AQUIDs constructed upon a ring-shaped optical lattice interrupted by a weak link has been proved to yield an effective two-level quantum dynamics able to reproduce a qubit [14]. Later, it was shown that the same lattice confinement, but interrupted by three weak links, also reproduces an effective qubit dynamics, but in a considerably enlarged parameter space [15]. Such efforts are opening the way towards an experimental realization of a cold atom analog of the superconducting flux qubit [16].

From the theoretical point of view, the modelization of AQUIDs has mostly been addressed by one-dimensional (1D), i.e., tight-waveguide, descriptions for which the Lieb-Liniger model generalized to host barrier potentials can be applied [17,18]. Different methods depending on the interaction strength have been utilized to study these systems. In the limit of weak interactions, the relevant physics of the system can be captured within the mean-field approximation by the Gross-Pitaevskii (GP) equation [14,18,19], whereas in the hard-core limit of infinite repulsion the Tonks-Girardeau Bose-Fermi mapping often provides analytic solutions [14,17,18]. For interaction strengths outside the above limits, one may resort to various computational techniques, such as several kinds of Monte Carlo approaches [17] and, in case of ring lattices, exact diagonalization schemes for small systems and the density-matrix renormalization group for larger system sizes [14,17]. Another useful approach comes from the quantum phase model, which assumes a system dynamics characterized by the phase differences across each junction, neglecting the site number fluctuations [14,20].

In the case of nonrotating double-well systems, a two-mode (TM) model was developed in Refs. [21,22] and latterly

improved by considering terms that gave rise to novel parameters [23]. We will focus in this paper particularly on one of such parameters, which has shown to provide almost vanishing effects in the nonrotating context. Given that a discrepancy still persisted between the model results and the GP simulations, an effective TM model was developed in recent years [24]. Such a model arises from introducing in the derivation of the equations of motion the on-site interaction energy dependence on the population imbalance. When doing so, one obtains the same type of equations, but with an effective interaction energy parameter instead of the standard on-site interaction one. In the Thomas-Fermi approximation, it has been shown that the effective interaction energy parameter becomes reduced with respect to the standard one by a factor of 7/10, 3/4, or 5/6, depending on the dimensionality of the system. Such an effective TM model has been shown to accurately describe the exact dynamics in double-well [24,25], asymmetric two-well [26,27], and, in the multimode version, multiple-well [28,29] condensates.

A multimode model, which includes all the types of corrections introduced in the TM model, was recently proposed for describing the dynamics of cold atoms confined by a rotating ring-shaped optical lattice forming a weakly linked array of condensates [30]. The on-site localized functions were obtained by means of a change of basis from that formed by the stationary order parameters with different winding numbers. Due to the rotation, the localized functions acquire a phase gradient along the bulk, which causes the formation of a phase difference across the junctions of neighboring localized functions. It has been shown that such a phase difference turns out to determine the argument of the complex hopping parameters.

In this paper, we will apply the above multimode model restricted to a double-well system in the form of a rotating TM version. Even though all the model parameters will be shown to be real numbers in this case, we will see that the phase gradient imprinted on the on-site localized functions, similarly to the multiwell case, plays a crucial role in determining the behavior of the hopping amplitudes as functions of the frequency. In particular, we will see that there exist frequencies where the standard hopping amplitudes vanish, and a usually disregarded parameter for nonrotating systems turns out to define the dynamics. Such a parameter, which in the nonrotating case is defined as proportional to the integral of the product of the densities of both localized functions, splits for the rotating condensate into two different model parameters, one of which is of a hoppinglike nature, playing an essential role, while the other is of interactionlike character, yielding negligible corrections.

One goal of this paper consists in showing that in correspondence with the increment of the role played by such a hopping parameter, the system exhibits the coexistence of two Josephson oscillation modes. In particular, we show that at the extremes of the frequency interval where both modes coexist, bifurcations of the stationary points take place. Thus, we analyze the way in which rotation affects the values of the model parameters, and further elucidate how such parameters modify the phase portrait and time periods. Such essential insights provided by the TM model are tested against GP simulations, which confirm that we are dealing with a simple

and quite accurate theoretical tool accounting for the response to rotation of a dc-AQUID.

This paper is organized as follows. In Sec. II we describe the system and details of the GP simulations we have performed. Section III deals with the rotating TM model, where we analyze the phase gradient on the on-site localized functions and derive the equations of motion in Sec. III A, while the dependence of the model parameters on the rotation frequency is discussed in Sec. III B. The phase portrait is described in Sec. IV, where we study the distribution of stationary points with their possible bifurcations in Sec. IV A, whereas the corresponding different types of phase portraits, particularly those presenting a coexistence of Josephson modes, are analyzed in Sec. IV B. Section V is devoted to examine the dynamics of orbits on the different regimes. We pay special attention to the time periods of both Josephson modes, deriving an analytical expression in the small-oscillation (SO) approximation. All the evolutions are compared to time-dependent GP simulations. Some concluding remarks are gathered in Sec. VI. Finally, useful alternative calculations of the hopping parameters are summarized in the Appendix.

II. THEORETICAL FRAMEWORK

We describe in what follows the condensate we have considered in our study, which was experimentally realized as AQUIDs in Refs. [7,12]. The trapping potential can be written as the sum of a term depending on x and y and a term that is harmonic in the tightly bound direction z :

$$V_{\text{trap}} = V(x, y) + \lambda^2 z^2 / 2 \quad (1)$$

with

$$V(x, y) = V_0 \left[1 - \left(\frac{r^2}{r_0^2} \right) \exp \left(1 - \frac{r^2}{r_0^2} \right) \right] + V_b \exp \left(-y^2 / \lambda_b^2 \right). \quad (2)$$

The above potential consists of a superposition of a toroidal term modeled through a Laguerre-Gauss optical potential [31], where V_0 corresponds to the potential depth and r_0 is the radial position of its minimum ($r^2 = x^2 + y^2$), and a Gaussian barrier along the x axis of height V_b and width λ_b that splits the torus into two halves, the one on the upper-half plane labeled as the “ u ” site and the other located on the lower-half plane, named the “ l ” site. The following system parameters were considered [12]: $V_0 = 70$ nK, $r_0 = 4 \mu\text{m}$, $V_b = 41$ nK, $\lambda_b = 1 \mu\text{m}$, and $N = 3000$ atoms of ^{87}Rb . We have also assumed a relative high value of λ , $18.8 \text{ nK}^{1/2} \mu\text{m}^{-1}$, which yields a quasi-bi-dimensional condensate. Thus, the condensate order parameter is written as the product of a Gaussian wave function along the z coordinate, and a two-dimensional (2D) wave function $\psi(\mathbf{r}, t)$ normalized to one, for which the corresponding GP equation in a rotating frame at the angular velocity $\Omega \hat{\mathbf{z}}$ reads [32]

$$[\hat{H}_0 + gN|\psi(\mathbf{r}, t)|^2 - \Omega \hat{L}_z] \psi(\mathbf{r}, t) = i\hbar \frac{\partial \psi(\mathbf{r}, t)}{\partial t}, \quad (3)$$

where $\hat{H}_0 = -\frac{\hbar^2}{2m} \nabla^2 + V$ is the noninteracting Hamiltonian, \hat{L}_z denotes the z component of the angular momentum operator, and g corresponds to the effective 2D coupling constant

between the atoms [32]. Such a GP equation has been numerically solved using the split-step Crank-Nicolson algorithm for imaginary- and real-time propagation on a 2D spatial grid of 257×257 points [33].

III. ROTATING TWO-MODE MODEL

A. On-site localized functions and equations of motion

In our TM model, the condensate order parameter $\psi_{\text{TM}}(\mathbf{r}, t)$ is written in terms of a pair of order parameters, which, by analogy with multiple-well systems, will be referred to as “on-site” localized functions. Therefore, the barriers being localized along $y = 0$ [Eq. (2)], we have an “upper” and a “lower” localized function, $\psi_u(\mathbf{r})$ and $\psi_l(\mathbf{r})$, respectively, from which the condensate order parameter is built as

$$\psi_{\text{TM}}(\mathbf{r}, t) = b_u(t)\psi_u(\mathbf{r}) + b_l(t)\psi_l(\mathbf{r}), \quad (4)$$

with $b_k(t) = \sqrt{N_k(t)/N} \exp[\varphi_k(t)]$ ($k = u, l$), where $N_k(t)$ represents the number of particles at the site k and $\varphi_k(t)$ denotes a global phase that takes into account the time dependence of the phase on that site [30]. Note that the spatial coordinate dependence of the condensate order parameter stems from those of the on-site localized functions. These are complex functions, the phases of which, respectively, denoted as $\phi_u(\mathbf{r})$ and $\phi_l(\mathbf{r})$ for the upper and lower localized functions, will be discussed below. In the nonrotating case, the localized functions arise from the sum and difference of the lowest-energy stationary order parameters obtained from the GP equation, i.e., the ground state with winding number $n = 0$ and the antisymmetric state, which for our toroidal configuration corresponds to a winding number $n = 1$ [28]. We note that the stationary order parameter of maximum winding number for nonrotating ring lattices, with an even number of sites, is characterized by presenting nodal surfaces along the barriers. The phase is homogeneous in each site, except at the junctions where a π phase difference exists. Hence, the uniform phases alternate between zero and π in consecutive sites. In our case the two-site lattice has a maximum winding number of 1, and hence the associated order parameter has the same behavior as an antisymmetric one.

For a finite angular frequency Ω , one may first calculate the rotating stationary order parameters ψ_0 and ψ_1 of winding numbers 0 and 1, respectively, by imaginary-time propagating through the GP equation (3) the corresponding nonrotating stationary states. It is worthwhile noticing that the total phase difference of ψ_1 around the torus is now distributed not only in the junctions but also in the bulk. Since such states have different initial winding numbers, the imaginary-time propagation keeps the orthogonality between them. This represents an important feature, as it determines the conservation of the two-state orthonormal basis in the rotating configuration. We may obtain the basis formed by the on-site localized functions as the sum and difference of the rotating stationary order parameters ψ_0 and ψ_1 . It is important to note that in order to achieve a maximum localization, such stationary states should have their phases previously fixed to zero at the middle of a site [29], which we have chosen to be the upper one, and at the point ($x = 0; y = r_0$). Such an ansatz for obtaining the localized functions corresponds to that of a rotating ring-shaped

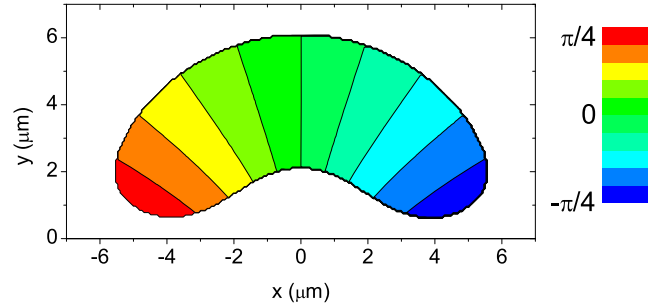


FIG. 1. Isodensity contour of the on-site localized function of the upper site $\psi_u(\mathbf{r})$ and its corresponding phase $\phi_u(\mathbf{r})$ for the frequency $f = \Omega/2\pi = 3.54$ Hz. The color scale corresponds to the phase of the function, while the contour corresponds to $1/14$ of the maximum value of $|\psi_u|^2$.

optical lattice described in Ref. [30], applied in this case to a two-well system.

Given that the bulks of the rotating stationary states acquire a phase gradient around the condensate, a phase with the same behavior is imprinted on the corresponding localized functions, as observed in Fig. 1. The upper localized function shown in this figure corresponds to the sum of both stationary states. In Figs. 2(a) and 2(b) we further show the phase and density of the stationary states ψ_0 and ψ_1 as functions of the angular coordinate θ , at $r = r_0$, for the frequency $f = \Omega/2\pi = 3.54$ Hz. In Fig. 2(c) we show the phases, $\phi_u(\theta)$ and $\phi_l(\theta)$, for the corresponding localized functions, together with the square amplitude of the upper localized function. There it may be seen that a phase difference $\Delta\phi_u = \pi/2$ exists between $\theta = 0$ and π of such localized function. To qualitatively explain such a value, it is useful to reduce the treatment of our system to a rotating 1D annulus of radius $r_0 = 4 \mu\text{m}$ with negligible barrier widths. In such a case, any fluid element should move with an angular velocity Ω , and hence the phase difference between the ends of each semicircle yields the 1D prediction $\Delta\phi_{1\text{D}} = \pi\Omega r_0^2 m/\hbar$. Then, for this simplified model, the $\pi/2$ difference should be attained for a rotation frequency of 3.6 Hz. On the other hand, in our more realistic extended system, the velocity field verifies the superfluidity condition and then acquires a more complex form [30]. Hence, we have found that the phase difference of $\pi/2$ is attained at the slightly smaller frequency of 3.54 Hz, with respect to the 1D prediction. We will see that such a phase difference on the on-site localized functions involves the presence of a related phase difference at the junctions. First, we note that it is easy to verify that the stationary state with winding number $n = 0$ corresponds to the TM order parameter (4) with vanishing global phases and equal populations $N_u = N_l$. However, in spite of the vanishing global phases, in Fig. 2(a) an extra negative phase difference can be appreciated at the junctions, which will be denoted as Θ . In order to obtain a quantized velocity field circulation around the torus, such a phase should verify $\Theta = -\pi/2$, which for any frequency can be generalized to $\Theta = -\Delta\phi_u$. With the purpose of better visualizing the precision of the Θ value in Fig. 2(d), we show as a solid line the phase of the TM order parameter (4) for global phases $\varphi_u = \pi/2 = -\Theta$ and $\varphi_l = 0$ with identical populations at each site. It may be seen that the discontinuity

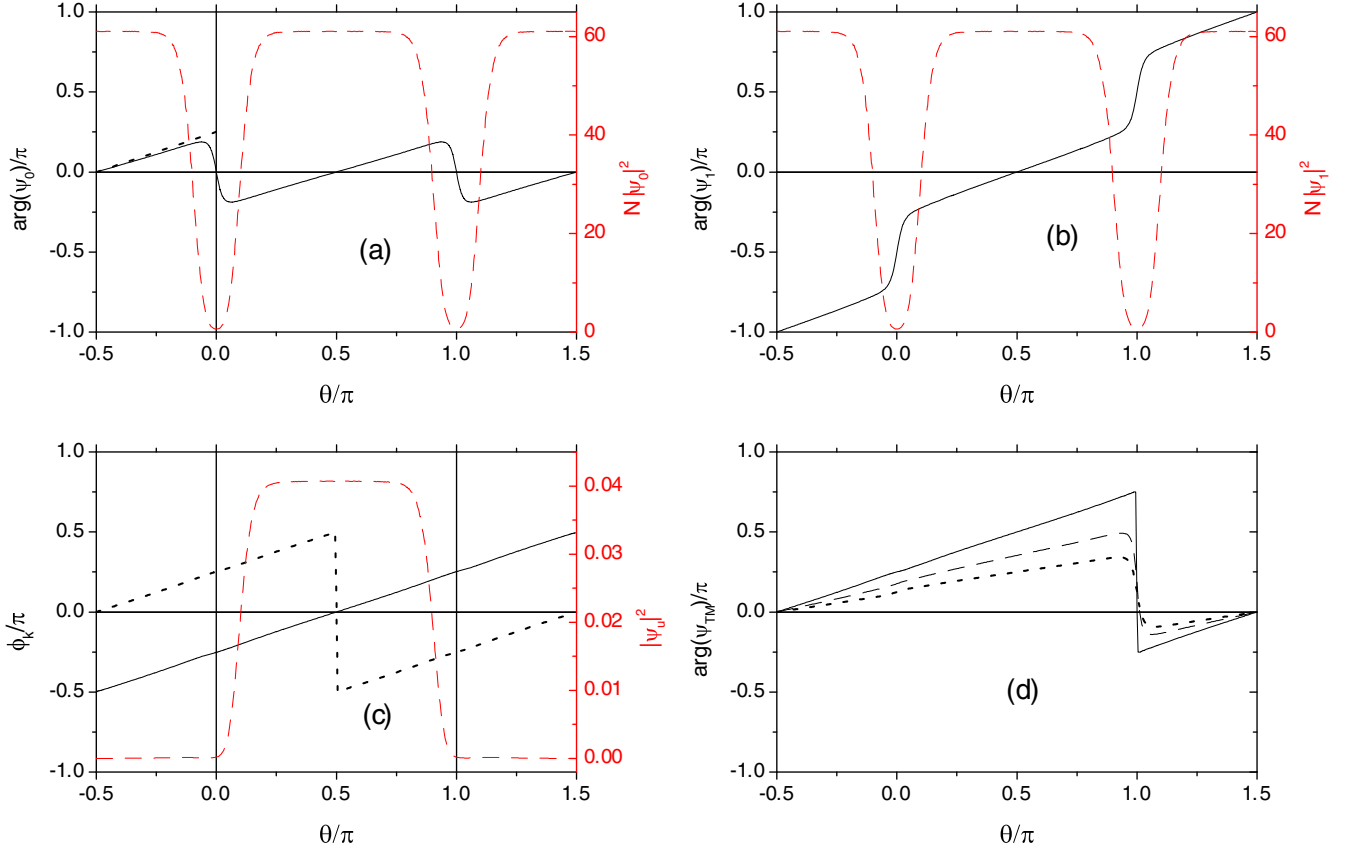


FIG. 2. (a) Phase (black solid line) and density (red dashed line) of the stationary state ψ_0 of winding number zero for the condensate rotating at the frequency $f = \Omega/2\pi = 3.54$ Hz. The dotted line displays the tangent to the phase at $\theta/\pi = -0.5$, the intersection of which with the solid vertical line indicates half of the phase difference across the junction. Such a vertical solid line shows the location of the right junction. (b) Solid and dashed lines: Same as panel (a) for the stationary state ψ_1 of winding number 1. (c) Phase ϕ_u of the upper (solid line) and lower ϕ_l (dotted line) on-site localized functions derived from the above stationary states. The red dashed line corresponds to the square amplitude of the upper localized function, while the solid vertical lines show the location of the junctions. (d) Phase of the TM order parameter (4) with the global phases $\varphi_u = -\Theta$ and $\varphi_l = 0$ and equal populations for three rotation frequencies: 3.54 Hz (solid line), 2.5 Hz (dashed line), and 1.77 Hz (dotted line).

disappears indeed at the right junction ($\theta = 0$), whereas a phase of $-\pi$ is present at the left junction, as expected. The same procedure was applied to two other rotation frequencies, showing that the phase difference at the right junction cancels indeed. For these two frequencies we have assumed a linear dependence for $-\Theta(f)$, with $\Theta(3.54 \text{ Hz}) = -\pi/2$, although, in practice, such a slope presents a small increment with the frequency, and hence this approximation can only be taken locally. The importance of presence of the phase Θ will become evident when analyzing the behavior of the TM model hopping parameters.

Finally, by inserting the order parameter (4) in the GP equation (3), we may extract after some algebra the TM equations of motion in terms of the particle imbalance $Z = (N_l - N_u)/N$ and the global phase difference between both sites of the condensate $\varphi = \varphi_u - \varphi_l$:

$$\hbar \frac{dZ}{dt} = -2K\sqrt{1-Z^2} \sin \varphi + \varepsilon(1-Z^2) \sin 2\varphi, \quad (5)$$

$$\hbar \frac{d\varphi}{dt} = Z \left[NU_{\text{eff}} + \frac{2K}{\sqrt{1-Z^2}} \cos \varphi - \varepsilon \cos 2\varphi - 2\varepsilon' \right]. \quad (6)$$

Here the TM model parameters are defined as follows [21–25]:

$$J = - \int d^2r \psi_u^* (\hat{H}_0 - \Omega \hat{L}_z) \psi_l, \quad (7)$$

$$F = -gN \int d^2r \psi_u^* |\psi_u|^2 \psi_l, \quad (8)$$

where J and F denote the standard and interaction-driven hopping parameters, respectively, the sum of which yields the full hopping amplitude K . The remaining parameters are

$$U = g \int d^2r |\psi_u|^4, \quad (9)$$

$$\varepsilon = gN \int d^2r (\psi_u^* \psi_l)^2, \quad (10)$$

$$\varepsilon' = gN \int d^2r |\psi_u|^2 |\psi_l|^2. \quad (11)$$

The effective on-site interaction parameter U_{eff} in Eq. (6) arises from considering U in Eq. (9) as a function of the imbalance. Such an effective parameter can be written as $U_{\text{eff}} = (1 - \alpha)U$, where the procedure to calculate α for an

arbitrary number of particles is explained in Refs. [25,28]. The Thomas-Fermi prediction [24] represents a lower bound for the $1 - \alpha < 1$ value. On the other hand, ε and ε' , respectively, denote the correlated hopping amplitude and the intersite interaction parameter. We have adopted the above denominations for the hopping parameters in accordance with Ref. [23], where it is shown that the second-quantized version of their improved (nonrotating) TM model has a term stemming from a nonvanishing value of $\varepsilon = \varepsilon'$ that contains correlated hopping or two-particle tunneling [34] effects, whereas what we have called the full hopping amplitude K only involves one-particle processes. It is worthwhile noticing that when the system is subject to rotation, the on-site localized functions are intrinsically complex, and hence one can identify a pure interaction parameter and a hopping amplitude, which are given by Eqs. (11) and (10), respectively. In contrast, we recall that in the nonrotating case a single parameter is obtained, since for real localized functions such expressions coincide. We note that in the derivation of Eqs. (5) and (6), we have used the fact that for a double-well condensate all the model parameters turn out to be real, as will be shown in the next subsection.

B. TM model parameters

For a rotating ring-shaped lattice with a number of sites larger than 2, the parameters J , F , and ε become complex numbers, the phases of which are related to the imprinted phase on the localized sites [30]. However, when only two sites with two junctions are considered, it is easy to verify that such parameters are real numbers. For instance, calling J_{ul} the parameter defined by Eq. (7), where the subscripts correspond to the order of the localized functions in the integrand, and taking into account that \hat{H}_0 and \hat{L}_z are Hermitian operators, we have $J_{ul}^* = J_{lu}$. On the other hand, as a result of the symmetry of the system, we have that the hopping amplitude must verify $J_{ul} = J_{lu} = J$ and, hence, $J_{ul}^* = J_{ul}$. The same analysis can be applied to the remaining parameters, F , ε , and K .

A strong dependence on the rotation frequency is expected for those parameters that depend on the imprinted phase of the localized functions. Such is the case for K and ε , which are depicted as functions of the frequency in Fig. 3. The relative values of these parameters will become crucial in determining the nature of the stationary points on different frequency intervals.

In order to qualitatively explain the behavior of K and ε as functions of the frequency, one can separately analyze the origin of both terms at the right-hand side of the equation of motion (5). First, we may consider that \dot{Z} has two contributions coming from the currents, I_L and I_R , flowing through the left and right junctions, respectively. In turn, each current has, in analogy with a single junction double-well system, two terms, one current $I_i^{(1)}$ proportional to $\sin(\varphi_i)$, and the other current $I_i^{(2)}$ proportional to $\sin(2\varphi_i)$, where φ_i denotes the phase difference at the right ($i = R$) and left ($i = L$) junctions, respectively. In view of the fact that, as described in the previous subsection, an additional phase difference Θ appears at each junction, we obtain that the phase differences at each junction are $\varphi_R = \varphi + \Theta$ and $\varphi_L = \varphi - \Theta$. Hence, denoting as \dot{Z}_1 the time derivative of the imbalance due to the sum of

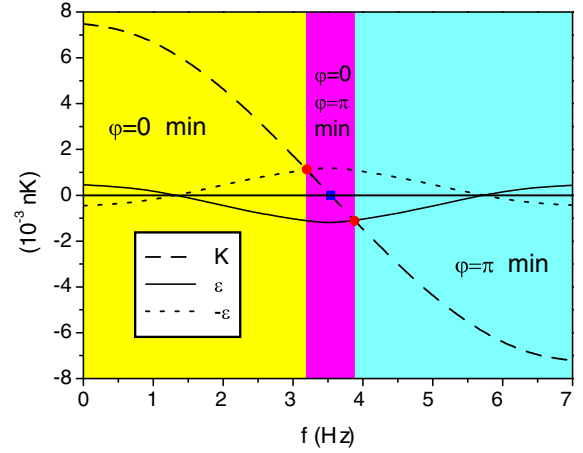


FIG. 3. TM parameters K and ε vs the rotation frequency $f = \Omega/2\pi$. The three frequency intervals indicated with different colors (grayscale values) correspond to qualitatively distinct phase-space portraits, which are characterized by the number and position of the energy minima. The intersection points $K = \pm\varepsilon$ (red circles) define the bifurcation frequencies $f_1 = 3.18$ Hz and $f_2 = 3.90$ Hz which determine the limits of the central frequency interval where coexist two energy minima at $\varphi = 0$ and π . At the central frequency (3.54 Hz), where $K = 0$ (denoted by a blue square), such minima possess the same depth. The remaining two frequency intervals, $f < f_1$ and $f > f_2$, exhibit a single minimum, as indicated in the drawing.

the currents $I_R^{(1)}$ and $I_L^{(1)}$, we have

$$\dot{Z}_1 \propto \sin(\varphi + \Theta) + \sin(\varphi - \Theta) = 2 \cos(\Theta) \sin(\varphi). \quad (12)$$

Since \dot{Z}_1 stems from the term of Eq. (5) proportional to K , we may conclude that the parameter K should be modulated by $\cos(\Theta)$, and the same modulation should apply for J and F .

Analogously, we may obtain the time derivative of the imbalance \dot{Z}_2 due to the sum of the currents $I_R^{(2)}$ and $I_L^{(2)}$ as

$$\dot{Z}_2 \propto \sin[2(\varphi + \Theta)] + \sin[2(\varphi - \Theta)] = 2 \cos(2\Theta) \sin(2\varphi), \quad (13)$$

which added to \dot{Z}_1 yields, the total imbalance derivative $\dot{Z} = \dot{Z}_1 + \dot{Z}_2$. Thus, from Eqs. (13) and (5), we may conclude that the parameter ε should be modulated by $\cos(2\Theta)$.

One may further use the 1D approximation $-\Theta \simeq \Delta\phi_{1D} = \pi\Omega r_0^2 m/\hbar$ and define $f_0 = \hbar/(m2\pi r_0^2)$, from which we have $K \simeq B_K(f) \cos(f\pi/f_0)$ and $\varepsilon \simeq B_\varepsilon(f) \cos(2f\pi/f_0)$, where, as seen from Fig. 3, the amplitudes $B_i(f)$ are positive and do not vary substantially as functions of f . For our system, the linear relationship between Θ and f is less rigorous since its modulus has a slightly increasing slope, but, as seen from the graph, such an approximation certainly captures the main behavior.

In nonrotating systems, the parameters F and ε were first introduced by Ananikian and Bergeman [23] in order to improve the TM model; however, as discussed by the authors, the latter in general verifies $\varepsilon \ll K$. Hence, in most cases it is not taken into account, or at least it is only used to introduce small corrections [25]. In this paper the nonrotating value of ε turns out to be about an order of magnitude smaller than K .

The above modulation of K implies that it should vanish at $\Theta = -\pi/2$, which is attained for $f = 3.54$ Hz. On the other hand, at the same frequency, the hopping parameter ε should acquire its maximum absolute value. Then, we infer that around such Θ value, ε turns out to be the leading hopping parameter of the model. As a consequence of this effect, in the next section it will be shown that two energy minima coexist in the phase portrait in the vicinity of such a frequency. It is worthwhile noticing that the same type of phenomenon also occurs at, for instance, $\Theta = -3/2\pi$ for a rotation frequency of 10.54 Hz.

On the other hand, we have found that the parameters U and α remain almost constant when varying the rotation frequency, as also observed in a previous work [30]. In particular, we have utilized the values $U = 1.186 \times 10^{-2}$ nK and $1 - \alpha = 0.814$ for the whole frequency interval. Given that we have assumed a rather low number of particles, we could not make use of Thomas-Fermi estimates, and hence the value of α was numerically obtained, as described in Refs. [25,28]. We note that such a value lies in between the 1D and 2D Thomas-Fermi predictions.

Finally, we note that in the Appendix we discuss alternative formulas for obtaining the TM parameters K and ε , in addition to the above expressions (7), (8), and (10). There we show that in the case of ε , such alternative calculations can be used to provide results with a better accuracy.

IV. PHASE PORTRAIT

The equations of motion (5) and (6) can be written in Hamiltonian form as

$$\dot{Z} = -\partial H/\partial\varphi \quad \text{and} \quad \dot{\varphi} = \partial H/\partial Z, \quad (14)$$

where the classical Hamiltonian H depends on the canonical variables Z and φ as

$$H(Z, \varphi) = \left(\frac{NU_{\text{eff}}}{2\hbar} - \frac{\varepsilon'}{\hbar} \right) Z^2 - 2\frac{K}{\hbar} \sqrt{1-Z^2} \cos\varphi + \frac{\varepsilon}{2\hbar} (1-Z^2) \cos 2\varphi. \quad (15)$$

A. Stationary points

According to (14), the stationary points correspond to the condition of vanishing partial derivatives of the Hamiltonian with respect to the canonical variables. For a nonrotating condensate [21–25], given that $\varepsilon < K$, the stationary points consist of an energy minimum at $(Z = 0, \varphi = 0)$, a saddle at $(Z = 0, \varphi = \pi)$, and two maxima at $(Z \simeq \pm 1, \varphi = \pi)$. However, these maxima do not possess stationary state counterparts in the GP equation, and hence they present no physical interest. New features appear when the condensate is subject to rotation, as a consequence of the fact that the value of K decreases and the absolute value of ε can become larger than K (see Fig. 3). We will see that stationary point bifurcations occur at certain frequencies f_1 and f_2 , and in between them two energy minima coexist. In particular, the first bifurcation frequency $f_1 = 3.18$ Hz is attained where $K = -\varepsilon$, a condition which makes the second derivative $\partial^2 H/\partial\varphi^2$ vanish at $(Z = 0, \varphi = \pi)$. This gives rise to a bifurcation along the $Z \equiv 0$ axis of the kind $s \rightarrow 2s + m$, where s denotes a saddle

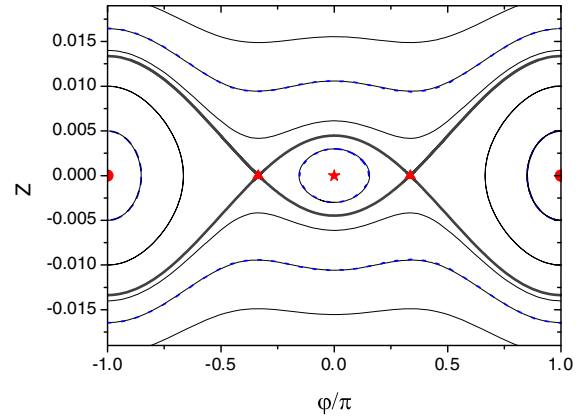


FIG. 4. Phase-space portrait Z vs φ arising from the Hamiltonian (15) for the rotation frequency $f = 3.72$ Hz. Each orbit is represented by a thin solid line, except for the separatrix that is depicted as a thick solid line. The circles and the star, respectively, represent the location of absolute and relative minima, while the triangles correspond to saddles. A very good agreement with a few selected orbits corresponding to GP simulations is observed (blue dashed lines).

and m a minimum. Then, at increasing frequencies, such a relative minimum stays at $\varphi = \pi$, while the saddles, located at $\varphi_s = \pm \cos^{-1}(K/\varepsilon)$, move in opposite directions along the $Z \equiv 0$ axis towards the point $\varphi = 0$. Particularly, when the saddles reach $\varphi = \pm\pi/2$ at the frequency of 3.54 Hz, the minima at $\varphi = 0$ and π have the same energy, whereas for larger frequencies the minimum at $\varphi = \pi$ acquires a lower energy than the minimum at $\varphi = 0$. Finally, at the second bifurcation frequency for which $\varepsilon = K$, $f_2 = 3.90$ Hz, the second derivative $\partial^2 H/\partial\varphi^2$ again vanishes, provoking a bifurcation of the type $2s + m \rightarrow m$. In other words, the saddles collapse at the origin, along with the relative minimum, yielding a single saddle at $\varphi = 0$ for larger frequencies, in addition to the minimum at $\varphi = \pi$.

We display in Fig. 4 the phase portrait for the rotation frequency $f = 3.72$ Hz, which belongs to the central interval of Fig. 3, located in between the bifurcation frequencies f_1 and f_2 . We may observe that it presents an absolute and a relative minimum at $\varphi = \pi$ and zero, respectively, and a couple of saddles at $\varphi_s = \pm \cos^{-1}(K/\varepsilon) \simeq \pm\pi/3$ ($\varepsilon \simeq 2K$ for this frequency).

B. Dynamical regimes on the different types of phase portraits

By following the premise that the position and character of each stationary point organize the dynamics, we may conclude from the above study that three topologically different types of phase portraits can be obtained, depending on in which range of values, defined by the bifurcation points, the rotation frequency lies. On the other hand, one can identify different regimes for each kind of phase portrait. For instance, we observe in Fig. 4 closed orbits around the minimum at the origin, which are referred to as zero modes. Analogously, the closed orbits around the minimum at $\varphi = \pi$ are called π modes. Both, the zero and π modes correspond to Josephson oscillation regimes. On the other hand, the open orbits with

a running phase not crossing the $Z \equiv 0$ axis belong to the macroscopic quantum self-trapping regime. Such a regime is separated from the Josephson regimes by the limiting orbit known as the separatrix. Such a curve serves as a boundary between different types of orbits and has been depicted as a thick solid line in Fig. 4. Since the separatrix has the energy of the saddle points, it is defined by the condition

$$H(Z, \varphi) = H(0, \varphi_s), \quad (16)$$

where H denotes the Hamiltonian (15). One can determine from the above equation the maximum particle imbalance Z_c that can be reached either in the zero or the π modes. In fact, in the low-frequency interval of Fig. 3 ($0 < f < f_1$), we have only zero modes ($\varphi = 0$) and a saddle at $\varphi_s = \pi$, which according to (16) and (15), and under the assumption that NU_{eff} is much larger than any other model parameter, yields

$$Z_c = \sqrt{\frac{8|K|}{NU_{\text{eff}}}}, \quad (17)$$

that is, the same expression obtained for the nonrotating case [25]. On the other hand, in the central frequency interval between the bifurcation values ($f_1 < f < f_2$), we have both zero and π modes, i.e., minima at $\varphi = 0$ and π , and saddles at $\varphi_s = \pm \cos^{-1}(K/\varepsilon)$. Thus, replacing such values in Eq. (16), we obtain the following expression for the critical imbalances Z_c^+ and Z_c^- of the zero and π modes, respectively:

$$Z_c^\pm = \sqrt{\frac{-2}{\varepsilon NU_{\text{eff}}}} (\varepsilon \mp K)^2. \quad (18)$$

Replacing in the above expression the parameter values corresponding to the phase portrait of Fig. 4, one obtains a quotient $Z_c^-/Z_c^+ = 3$, which turns out to be in accordance with the separatrix values at $\varphi = \pi$ and zero, as seen in the graph. Finally, it is easy to show that the critical imbalance for the π modes of the last frequency interval, $f > f_2$, in Fig. 3, is again given by the expression (17). We note that it is straightforward to verify that Eqs. (17) and (18) coincide at the bifurcation frequencies, as expected. Such theoretical predictions, which show an excellent agreement with the GP simulation results, are depicted in Fig. 5.

V. DYNAMICS

First, it is interesting to analyze the impact that both the correlated hopping and the intersite interaction parameters, have on the time periods when varying the rotation frequency. In the nonrotating case, a system for which such a correction ($\varepsilon = \varepsilon'$) cannot be neglected was recently considered [25]. There it was shown that the main effect was restricted to low imbalances in the Josephson regime. That is, such a correction turned out to be appreciable only in the SO limit, with a decreasing incidence for increasing particle imbalances up to the critical value and negligible effects in the self-trapping regime. In the present rotating case, we will focus on the SO approximation for the time periods, which is expected to be deeply modified at frequencies where ε becomes of the order

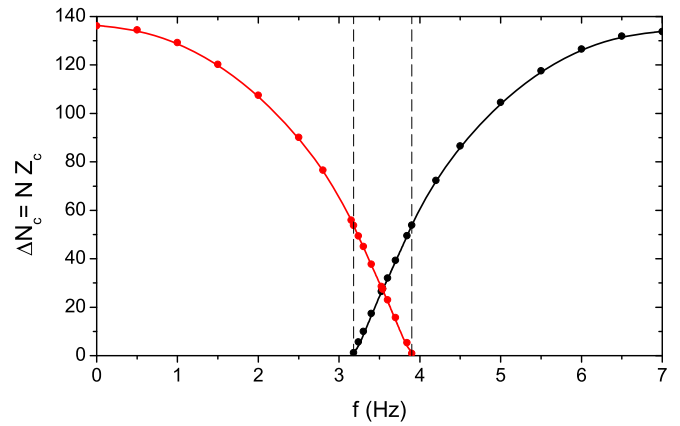


FIG. 5. Critical particle imbalance vs the rotation frequency. The vertical dashed lines indicate the bifurcation frequencies, which separate the three frequency intervals of Fig. 3. The circles denote the values of GP simulation results, while the full lines correspond to the theoretical predictions (17) and (18). The results belonging to zero modes (π modes) are depicted in red (black).

of K . Then, by linearizing the equations of motion we obtain

$$T_\pm = \frac{\pi \hbar}{\sqrt{(\pm K - \varepsilon)(NU_{\text{eff}}/2 \pm K - \varepsilon/2 - \varepsilon')}}, \quad (19)$$

where T_+ (T_-) denotes the SO period of the zero (π) modes. We note that the above formula for T_+ reduces to the one previously obtained in Ref. [25] for a nonrotating condensate by taking $\varepsilon = \varepsilon'$. Given that NU_{eff} turns out to be much greater than the remaining parameters, the intersite interaction has a negligible effect on (19). On the other hand, divergencies of the period occur at the bifurcation frequencies due to the $(\pm K - \varepsilon)$ factor in the denominator. In Fig. 6, we display the results arising from Eq. (19) (solid lines), together with the corresponding results for vanishing values of ε and ε' (dashed lines). Thus, we may observe that for the condensate without rotation, the period does not differ appreciably from that of the $\varepsilon = \varepsilon' = 0$ case, as happens for most nonrotating

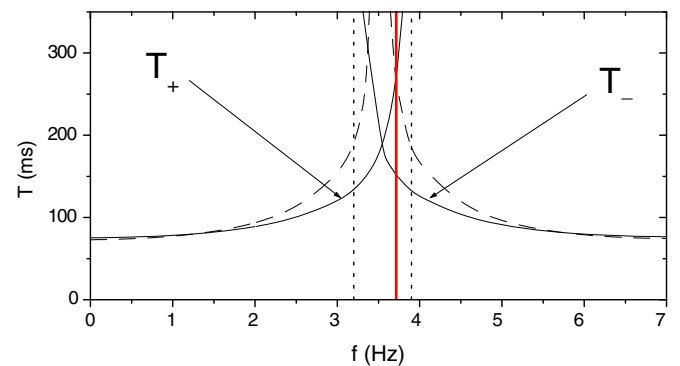


FIG. 6. SO periods T_+ and T_- given by Eq. (19) vs the rotational frequency f (solid lines). The vertical dotted lines indicate the bifurcation frequencies which separate the three frequency intervals of Fig. 3. Within the central interval, the vertical red line corresponds to the frequency $f = 3.72$ Hz of the phase portrait of Fig. 4. We also depict as dashed lines the periods obtained from Eq. (19) with vanishing values of ε and ε' .

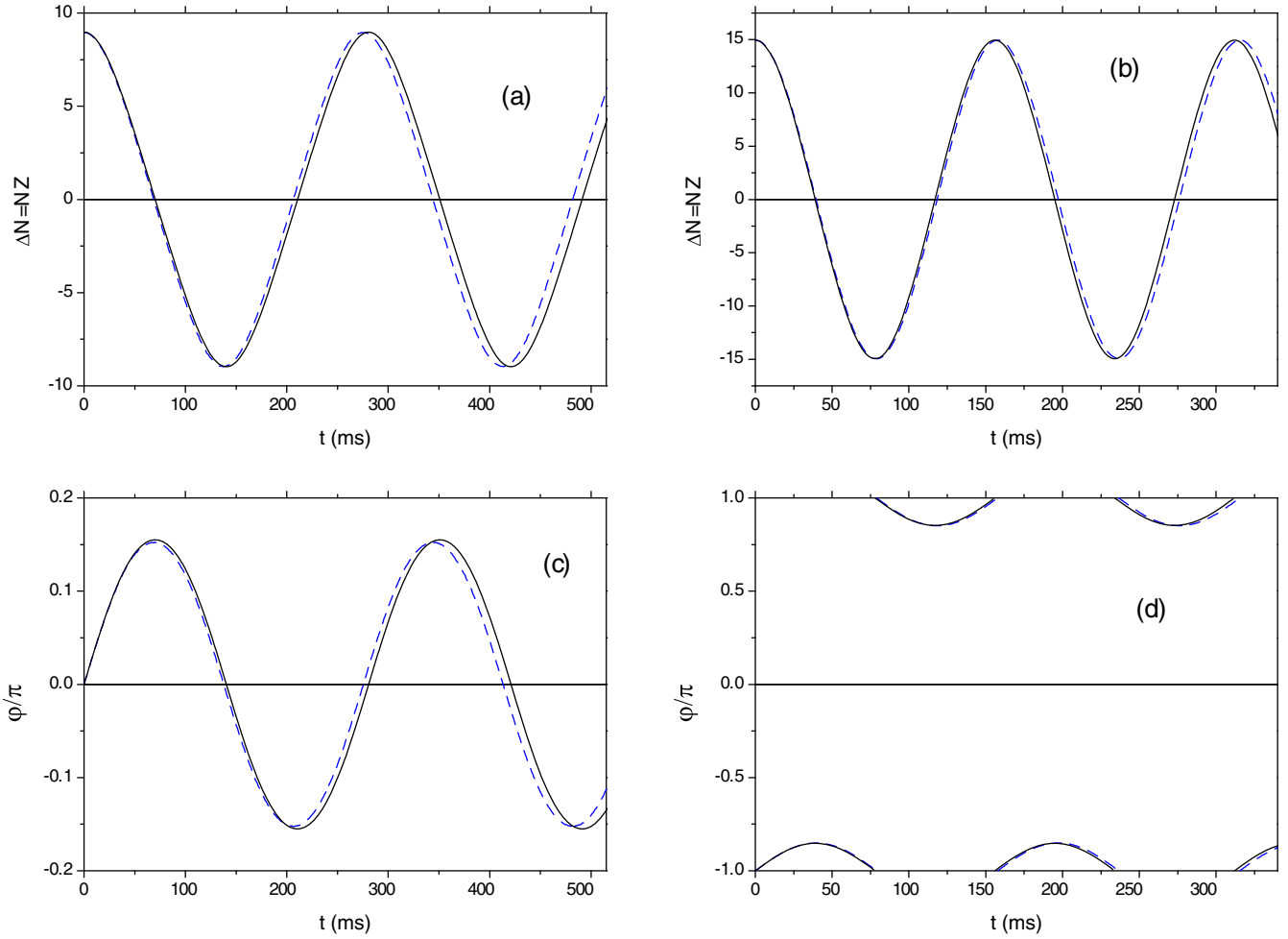


FIG. 7. Time evolution of the imbalance (a), (b) and phase difference (c), (d) for the Josephson modes of the condensate rotating at $f = 3.72$ Hz. Left (a), (c) and right (b), (d) panels show the zero and π modes, respectively. Black solid (blue dashed) lines correspond to TM model (GP simulation) results.

systems. In contrast, for the rotating condensate, even out of the two-minimum zone delimited by the bifurcation frequencies, there exists a sizable difference between the dashed and solid lines in Fig. 6. Particularly, above $f = 2$ Hz such a separation between lines becomes very visible, reflecting the incidence of the correlated hopping on the period. Time evolutions of particle imbalance and phase difference for initial conditions within the Josephson and self-trapping regimes are shown in Figs. 7 and 8, respectively. We have considered the case of the rotation frequency 3.72 Hz, the phase-space portrait of which was discussed in Sec. IV. The left panels of Fig. 7 show the evolutions obtained from the TM model and the GP simulations for the zero-mode Josephson orbit depicted in Fig. 4, whereas the corresponding evolutions of the π mode of the smaller orbit are shown on the right panels. We note that the time periods in the SO approximation for the present frequency (marked with a vertical red line in Fig. 6) are around $T_+ \simeq 250$ ms and $T_- \simeq 150$ ms, for the zero and π modes, respectively. Such values can be considered as rough estimates of the periods of Fig. 7, where we observe a closer estimate for the π mode, despite its larger initial imbalance. This is due to the fact that such an orbit lies farther from the separatrix than the zero mode. Actually, it has been shown in

Ref. [25] that the SO periods constitute lower bounds of the Josephson periods, which, on the other hand, diverge when approaching the critical imbalance.

Finally, Fig. 8 displays the time evolution of particle imbalance and phase difference for the self-trapping orbit of Fig. 4 with the initial conditions $Z(0) = 0.017$ and $\varphi(0) = -\pi$. We may see that the imbalance presents peaks of absolute and relative maxima corresponding to $\varphi = \pm\pi$ and zero, respectively, which is in accordance with having a larger Z_c for the π mode than that of the zero mode, as shown in Fig. 5. Given that also in the self-trapping regime the dominant term of the right-hand side of Eq. (6) is the first one, one can approximate the period as $T_{ST} = 2\pi\hbar/(\langle Z \rangle NU_{\text{eff}})$, where $\langle Z \rangle$ denotes the mean value of the imbalance over one period. Hence, the above modulation of the imbalance due to the role of the hopping amplitude ε indirectly affects the time period. In particular, the period observed in Fig. 8 is about 140 ms, which is consistent with $\langle Z \rangle N \simeq 35$.

To conclude we remark that a very good agreement between the TM model and the GP simulation results was observed for all the rotational frequencies we have explored, and the above exposed results may be taken as a representative example of such an accordance.

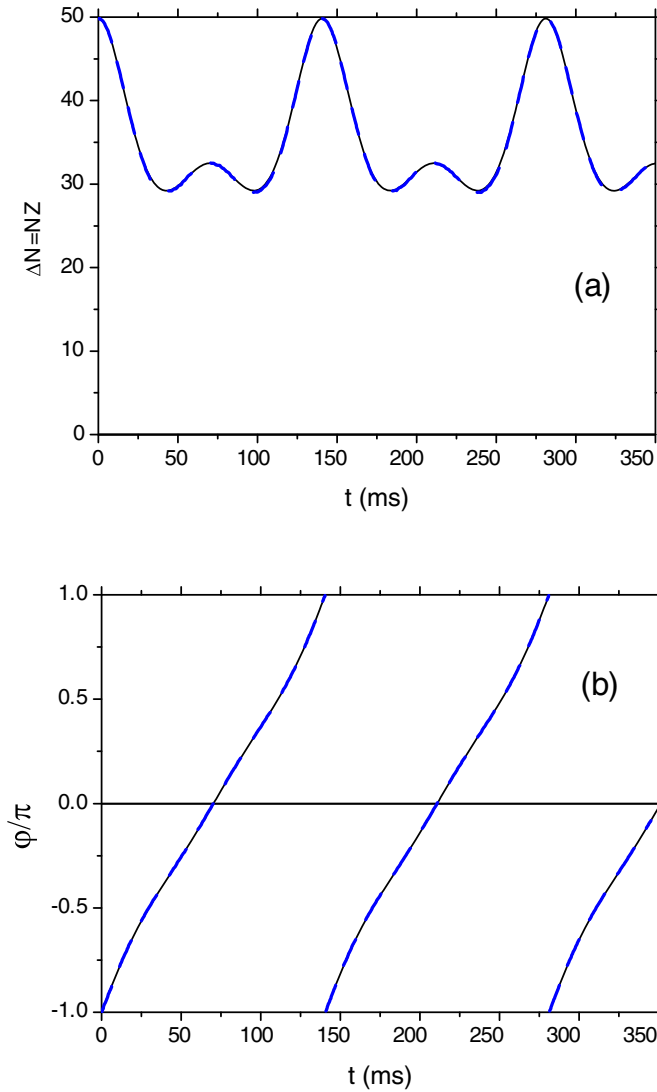


FIG. 8. Particle imbalance and phase difference vs time are shown in the upper (a) and lower (b) panel, respectively. The initial conditions $Z(0) = 0.017$ and $\varphi(0) = -\pi$ correspond to a self-trapping orbit in Fig. 3. The black solid and blue dashed lines correspond to the TM model and GP simulation results, respectively.

VI. CONCLUSION

We have shown that by rotating a toroidal-type double-well condensate, a much richer dynamics of the macroscopic conjugate coordinates can emerge, basically the coexistence of Josephson zero and π modes. Our findings have relied on a TM model suitable for such a rotating system. We have shown that the behavior of the hopping amplitudes K and ε with respect to rotation leads to an inversion of their relative strengths, as compared to the usual nonrotating relative values. Such parameters exhibit periodic modulations as functions of the rotational frequency, but, given that the period of one of them is one-half of the other, there exist crossings between such curves. In particular, at the frequencies where the absolute values of both hopping amplitudes coincide, bifurcations of stationary points in the phase space occur, which in turn give rise to the coexistence of two regimes of Josephson modes. We have shown that the frequency periods of

such parameters can be easily estimated using a 1D approach, which may be useful for designing a convenient experimental setup to reproduce this dynamics.

An extra benefit of having explored the rotation aspects of the system was to gain a more profound insight on the nature of the model parameters. Due to the phase gradient experimented by the on-site localized functions, we were able to distinguish between the hopping and interaction parameters ε and ε' , which are coincident in the nonrotating case. Moreover, as previously observed, such a correlated hopping can be related to the tunneling of pairs of particles, which suggests that the coexistence of Josephson modes could be a consequence of such tunneling processes.

To conclude, we have presented a simple and quite accurate bimodal model of the rotation dynamics of a dc AQUID, which can be regarded as an important advance to be employed to analyze the interference of persistent currents in atomtronic devices.

ACKNOWLEDGMENTS

D.M.J. and H.M.C. acknowledge CONICET for financial support under PIP Grant No. 11220150100442CO. H.M.C. acknowledges Universidad de Buenos Aires for financial support under UBA-CyT Grant No. 20020190100214BA.

APPENDIX: ALTERNATIVE CALCULATION OF THE TM PARAMETERS K AND ε

There is a simple relationship between the parameter K and the energy gap between both stationary states:

$$K = \Delta E/2, \quad (\text{A1})$$

where $\Delta E = E_1 - E_0$, with E_1 (E_0) the energy per particle of the stationary state with winding number $n = 1$ ($n = 0$) obtained from the GP equation. Equation (A1) provides a useful tool to test the accuracy of the TM model. For instance, if the potential barriers were not high enough, or the on-site functions were not properly localized, the energies E_1 and E_0 would not satisfy (A1) [29]. Then, we have utilized the above formula to test such accuracy of the K values obtained from the integrals (7) and (8), finding a coincidence within four digits along the whole frequency range of Fig. 3.

It is worthwhile noticing that the above winding numbers correspond to the nonrotating case, as they can change in amounts of two units at increasing angular velocities due to the discrete twofold rotational symmetry of the system [30]. For instance, the stationary state of winding number $n = 0$ acquires for frequencies approaching 7 Hz the value $n = 2$, whereas the stationary state of winding number $n = 1$ conserves this value for the whole frequency range shown in Fig. 3.

In Sec. V, the parameters ε and ε' were shown to be related according to Eq. (19) to the SO period arising from the Hamiltonian (15). Now, taking into account that we work with a NU_{eff} value which is three orders of magnitude larger than the remaining parameters K , ε and ε' , we may approximate (19) as

$$T_{\pm} = \pi \hbar \sqrt{\frac{2}{NU_{\text{eff}}(\pm K - \varepsilon)}}, \quad (\text{A2})$$

from which we may obtain the following expression,

$$\varepsilon = \pm K - \frac{2\pi^2 \hbar^2}{NU_{\text{eff}} T_{\pm}^2}, \quad (\text{A3})$$

which was in fact utilized to calculate the values of the parameter ε , given that it provides results of a much better accuracy than the numerical integration of expression (10).

-
- [1] L. Amico, M. Boshier, G. Birkel, A. Minguzzi, C. Miniatura, L.-C. Kwek, D. Aghalmalyan, V. Ahufinger, D. Anderson, N. Andrei *et al.*, *AVS Quantum Sci.* **3**, 039201 (2021); L. Amico, D. Anderson, M. Boshier, J.-P. Brantut, L.-C. Kwek, A. Minguzzi, and W. von Klitzing, [arXiv:2107.08561](https://arxiv.org/abs/2107.08561) (2021).
- [2] J. Clarke and A. I. Braginski, *The SQUID Handbook* (Wiley, New York, 2004); R. L. Fagaly, *Rev. Sci. Instrum.* **77**, 101101 (2006).
- [3] K. C. Wright, R. B. Blakestad, C. J. Lobb, W. D. Phillips, and G. K. Campbell, *Phys. Rev. Lett.* **110**, 025302 (2013).
- [4] S. Eckel, J. G. Lee, F. Jendrzejewski, N. Murray, C. W. Clark, C. J. Lobb, W. D. Phillips, M. Edwards, and G. K. Campbell, *Nature (London)* **506**, 200 (2014).
- [5] J. Dalibard, F. Gerbier, G. Juzeliunas, and P. Öhberg, *Rev. Mod. Phys.* **83**, 1523 (2011).
- [6] Y. Sato and R. E. Packard, *Rep. Prog. Phys.* **75**, 016401 (2012).
- [7] C. Ryu, E. C. Samson, and M. G. Boshier, *Nat. Commun.* **11**, 3338 (2020).
- [8] G. Pelegrí, J. Mompert, and V. Ahufinger, *New J. Phys.* **20**, 103001 (2018).
- [9] E. Nicolau, J. Mompert, B. Juliá-Díaz, and V. Ahufinger, *Phys. Rev. A* **102**, 023331 (2020).
- [10] P. Kumar, T. Biswas, K. Feliz, R. Kanamoto, M.-S. Chang, A. K. Jha, and M. Bhattacharya, *Phys. Rev. Lett.* **127**, 113601 (2021).
- [11] C. L. Degen, F. Reinhard, and P. Cappellaro, *Rev. Mod. Phys.* **89**, 035002 (2017).
- [12] C. Ryu, P. W. Blackburn, A. A. Blinova, and M. G. Boshier, *Phys. Rev. Lett.* **111**, 205301 (2013).
- [13] F. Jendrzejewski, S. Eckel, N. Murray, C. Lanier, M. Edwards, C. J. Lobb, and G. K. Campbell, *Phys. Rev. Lett.* **113**, 045305 (2014).
- [14] D. Aghalmalyan, M. Cominotti, M. Rizzi, D. Rossini, F. Hekking, A. Minguzzi, L.-C. Kwek, and L. Amico, *New J. Phys.* **17**, 045023 (2015).
- [15] D. Aghalmalyan, N. T. Nguyen, F. Auksztol, K. S. Gan, M. Martínez Valado, P. C. Condylis, L.-C. Kwek, R. Dumke, and L. Amico, *New J. Phys.* **18**, 075013 (2016).
- [16] L. Amico, D. Aghalmalyan, F. Auksztol, H. Crepaz, R. Dumke, and L.-C. Kwek, *Sci. Rep.* **4**, 4298 (2014).
- [17] M. A. Cazalilla, R. Citro, T. Giamarchi, E. Orignac, and M. Rigol, *Rev. Mod. Phys.* **83**, 1405 (2011).
- [18] J. Polo, R. Dubessy, P. Pedri, H. Perrin, and A. Minguzzi, *Phys. Rev. Lett.* **123**, 195301 (2019).
- [19] A. Pérez-Obiol, J. Polo, and T. Cheon, *Phys. Rev. A* **102**, 063302 (2020).
- [20] R. Fazio and H. van der Zant, *Phys. Rep.* **355**, 235 (2001).
- [21] A. Smerzi, S. Fantoni, S. Giovanazzi, and S. R. Shenoy, *Phys. Rev. Lett.* **79**, 4950 (1997).
- [22] S. Raghavan, A. Smerzi, S. Fantoni, and S. R. Shenoy, *Phys. Rev. A* **59**, 620 (1999).
- [23] D. Ananikian and T. Bergeman, *Phys. Rev. A* **73**, 013604 (2006).
- [24] D. M. Jezek, P. Capuzzi, and H. M. Cataldo, *Phys. Rev. A* **87**, 053625 (2013).
- [25] M. Nigro, P. Capuzzi, H. M. Cataldo, and D. M. Jezek, *Eur. Phys. J. D* **71**, 297 (2017).
- [26] H. M. Cataldo and D. M. Jezek, *Phys. Rev. A* **90**, 043610 (2014).
- [27] H. M. Cataldo, *Phys. Rev. A* **102**, 023323 (2020).
- [28] D. M. Jezek and H. M. Cataldo, *Phys. Rev. A* **88**, 013636 (2013).
- [29] M. Nigro, P. Capuzzi, H. M. Cataldo, and D. M. Jezek, *Phys. Rev. A* **97**, 013626 (2018).
- [30] M. Nigro, P. Capuzzi, and D. M. Jezek, *J. Phys. B* **53**, 025301 (2020).
- [31] E. M. Wright, J. Arlt, and K. Dholakia, *Phys. Rev. A* **63**, 013608 (2000).
- [32] Y. Castin and R. Dum, *Eur. Phys. J. D* **7**, 399 (1999).
- [33] R. K. Kumar, V. Lončar, P. Muruganandam, S. K. Adhikari, and A. Balaž, *Comput. Phys. Comm.* **240**, 74 (2019).
- [34] O. Dutta, M. Gajda, P. Hauke, M. Lewenstein, D.-S. Lühmann, B. A. Malomed, T. Sowiński, and J. Zakrzewski, *Rep. Prog. Phys.* **78**, 066001 (2015).